IEEE CSC & ESAS SUPERCONDUCTIVITY NEWS FORUM (global edition), September 2019.
Invited presentation 4-SQ-I-3 given at ISEC, 28 July-1 August 2019, Riverside, USA.

Towards Energy-Dispersive Particle Detection with sub-eV Energy Resolution: Metallic Magnetic Calorimeters with Direct Sensor Readout

Matthäus Krantz*, Andreas Fleischmann*, Christian Enss*, and Sebastian Kempf*
* Kirchhoff-Institute for Physics
Heidelberg University
Heidelberg, Germany
Email: sebastian.kempf@kip.uni-heidelberg.de

***Abstract*—Metallic magnetic calorimeters are energy-dispersive cryogenic particle detectors providing an excellent energy resolution, a fast signal rise time, a high quantum efficiency as well as an almost ideal linear detector response. To surpass the present record resolution of $1.6\,\mathrm{eV}$ (FWHM) for $6\,\mathrm{keV}$ photons, we have started to develop integrated detectors for which the paramagnetic temperature sensor monitoring the temperature rise of the detector is integrated directly into the pickup loop of the superconducting quantum interference device. Due to the greatly enhanced magnetic flux coupling and consequently the reduced contribution of SQUID noise to the overall noise spectrum, this kind of devices should push the resolution to a value well below $1\,\mathrm{eV}$. Here, we discuss the design and performance of a prototype 64 pixels metallic magnetic calorimeter based detector array with integrated detectors that rely on first-order parallel gradiometric SQUIDs with two meander-shaped pickup coils onto which planar temperature sensor made of Ag:Er are deposited.**

***Index Terms*—SQUIDs, X-ray detectors, Superconducting photodetectors, Ionizing radiation sensors**

I. Introduction

Metallic magnetic calorimeters (MMCs) are calorimetric low-temperature particle detectors that are presently strongly advancing the state-of-the-art in energy-dispersive single particle detection [1]. They are typically operated at temperatures well below $100\,\mathrm{mK}$ and make use of a metallic, paramagnetic temperature sensor to transduce the temperature rise of an absorber upon the impact of an energetic particle into a change of sensor magnetization. The latter can be precisely measured as a change of magnetic flux using a superconducting pickup coil that is coupled to a superconducting quantum interference device (SQUID). This outstanding interplay between a highly-sensitive magnetic thermometer and a near quantum-limited amplifier results in a fast signal rise time, an excellent energy resolution, a large energy dynamic range, a high quantum efficiency and an almost ideal linear detector response.

The temperature sensor of state-of-the-art MMCs is coupled to the SQUID via a superconducting flux transformer that is formed by a pickup coil inductively coupled to the sensor and the input coil of a current-sensing SQUID. However, parasitic inductances within this circuit as well as transformer losses due to a non-ideal magnetic coupling between different coils (the magnetic coupling factor k is usually below $100\,\%$) lead to a reduction of the actually measured signal size. In addition, SQUID noise becomes the dominant noise contribution for frequencies above several kilohertzes [1]. Both effects impair the achievable energy resolution of MMCs. A possible route to tackle these impairments is to use detectors with direct sensor readout for which the temperature sensor and the SQUID are combined in an integrated device, i.e. the sensor is placed inside the SQUID loop. This approach has already been shown very promising results [2]–[4]. However, these former devices had not been fully optimized, e.g. with respect to the detector geometry, and both the temperature sensor and the particle absorber were not fully microfabricated, thus significantly complicating to build large detector arrays.

We would like to thank T. Wolf and D. Nagler for technical support during device fabrication. The work was performed within the framework of the European Microkelvin Platform EMP and was supported by the BMBF grant 05P15VHFAA.

II. Detector geometry

Fig. 1 depicts the detector geometry used for the prototype detector array. It relies on a first-order parallel gradiometric SQUID those inductance is formed by two meander-shaped coils that are connected in parallel. A planar paramagnetic temperature sensor is placed onto each of these coils such that the change of sensor magnetization is directly changing the magnetic flux threading the SQUID loop. For both pixels, the particle absorber is placed above the temperature sensor and is connected to the sensor via normal conducting stems. The absorbers are hence free-standing and are supported only by tiny normal conducting structures in order to prevent a loss of athermal phonons during signal formation [1]. To generate the bias magnetic field required to induce a temperature dependent sensor magnetization, a persistent current is injected into a meander-shaped coil placed below the SQUID inductance. Utilizing two separate coils for bias and magnetization pickup allows to connect different field generating coils in series in order to inject a persistent current simultaneously in all detectors within the array. The use of a first-order parallel gradiometric SQUID cancels on one hand fluctuations of ho-

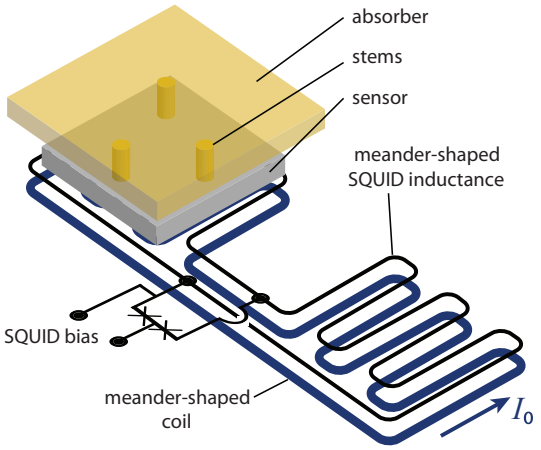

Fig. 1. Schematic of the detector geometry used for the prototype detector array. The SQUID is a first-order parallel gradiometer whose inductance is formed by two meander-shaped pickup coils onto which planar paramagnetic temperature sensors are placed. The particle absorbers are connected via normal conducting stems to underlying temperature sensor. A persistent current I_0 running inside meander-shaped coil underneath the SQUID loop is generating the bias magnetic field. For clarity, the temperature sensor, stems and absorber of the lower right meander-shaped coil as well as a feedback coil used for flux biasing the SQUID are not shown.

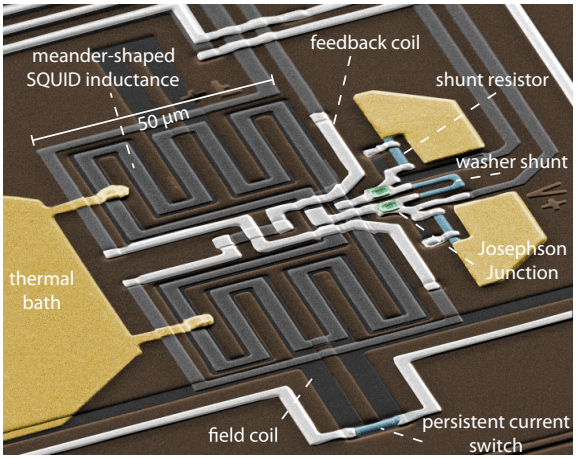

Fig. 2. **a)** Colored SEM picture of one of the detectors of the prototype detector array. The function of the different components is explained in the text. For making the picture, the paramagnetic temperature sensor, the stems as well as the particle absorbers of both pixels were not deposited.

mogeneous magnetic background fields and on the other hand cancels temperature fluctuations, e.g. of the heat bath, that affect both temperature sensors simultaneously. In addition, this detector configuration allows to read out two pixels by using only one SQUID since events in the different absorbers can be distinguished by the signal polarity.

III. Prototype Detector Array

Fig. 2 shows an SEM picture of one of the 32 detectors of the prototype array. The linewidth, pitch and area of each meander-shaped coil forming the SQUID inductance are $4\,\mu\mathrm{m}$, $10\,\mu\mathrm{m}$, and $50\,\mu\mathrm{m} \times 50\,\mu\mathrm{m}$. The inductance of each coil was numerically calculated and is $160\,\mathrm{pH}$, resulting in a total SQUID inductance of about $80\,\mathrm{pH}$. Each Josephson junction has a critical current of $I_\mathrm{c} = 6.3\,\mu\mathrm{A}$ and is shunted by a $4.5\,\Omega$ resistor made of AuPd. For thermalizing the shunts cooling fins are attached. A $9\,\Omega$ washer shunt is connected in parallel to both pickup coil to damp the SQUID LC resonance. A feedback coil is wound around the SQUID inductance to provide a flux bias and feedback.

The linewidth and pitch of the field generating meander-shaped coils are $6\,\mu\mathrm{m}$ and $10\,\mu\mathrm{m}$. They are separated from the SQUID inductance by a $300\,\mathrm{nm}$ thick insulation layer made of sputtered SiO_2. For injecting the persistent current, the coil has two extensions. On top of one these extensions, a resistor is placed that allows to drive the extension normal conducting to inject the persistent current into the coil.

The temperature sensor is made of Ag:Er with an erbium concentration of $450\,\mathrm{ppm}$ and is $1.2\,\mu\mathrm{m}$ thick. It is separated from the SQUID by a $300\,\mathrm{nm}$ thick insulation layer made of sputtered SiO_2. For sensor thermalization, an on-chip heat bath made of sputtered Au is connected via a small normal conducting stripe to each sensor. The dimensions of the stripes are chosen such that the decay time of the detector signals is about $0.6\,\mathrm{ms}$.

IV. Performance of Detector Array

For characterizing the detector array we mounted the array on a custom-made detector platform that was installed at the experimental platform of a commercial ^{3}He/^{4}He dilution refrigerator (BF-LD250, BlueFors Oy). Each of the detector SQUIDs was connected to a home-made 16-SQUID series array to form a two-stage SQUID setup. The SQUID arrays were read out using a directly coupled commercial SQUID electronics (XXF-1, Magnicon GmbH). The use of a two-stage SQUID setup first allows to voltage bias the detector SQUIDs to minimize the on-chip power dissipation of the SQUID that might affect the detector operation temperature and simultaneously allows to minimize the influence of the noise contribution of the SQUID electronics. At the same time, it increases the slew rate and the system bandwidth as compared to a flux modulation based SQUID readout. A flux-locked loop with flux feedback to the detector SQUID was used for linearizing the relation between the magnetic flux coupled into the SQUID loop and the output voltage of the SQUID electronics. For measuring the signal shape and height as well as to determine the energy resolution of the array, we irradiated the detector with X-ray photons emitted by an ^{55}Fe calibration source having two characteristic lines at about $5.9\,\mathrm{keV}$ and about $6.5\,\mathrm{keV}$. For all measurements discussed here, we used a field-generation persistent current of $I_0 = 160\,\mathrm{mA}$ and the temperature of the experimental platform was $7\,\mathrm{mK}$.

Fig. 3 shows the change of magnetic flux $\Delta\Phi_\mathrm{s}$ within the SQUID loop of one of the detectors versus time for a single detector event caused by the absorption of a $5.9\,\mathrm{keV}$ photon. The signal height is about $0.6\,\Phi_0$ and the signal decay can be described by an exponential decay with a decay time constant

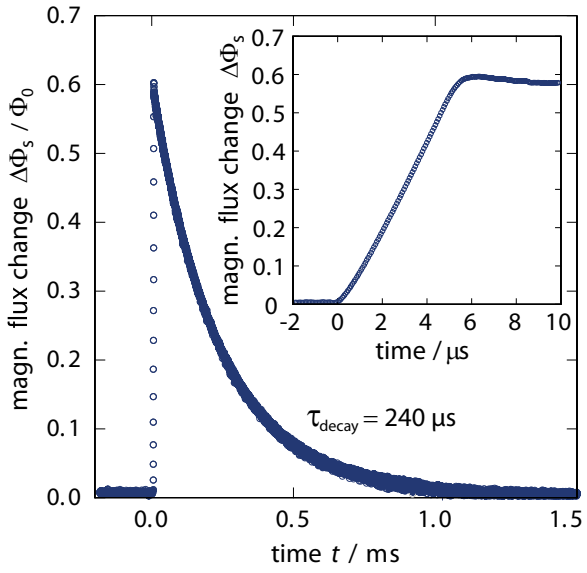

Fig. 3. Change of magnetic flux $\Delta\Phi_s$ within the SQUID loop versus time for a single detector event caused by the absorption of a $5.9\,\mathrm{keV}$ photon. The decay of the signal follows an exponential decay with a decay time constant of $\tau_{\mathrm{decay}} = 240\,\mu\mathrm{s}$. The inset shows a zoom into the signal rise which is linear rather than exponential. This indicates that slew rate of the SQUID readout limits the signal rise.

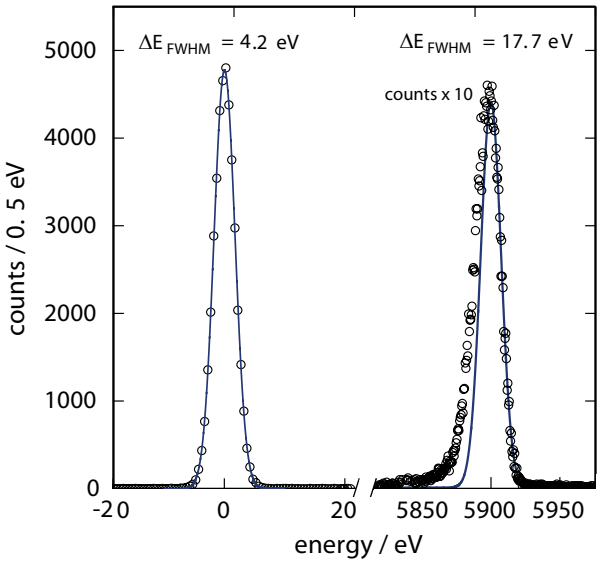

Fig. 4. Baseline spectrum as well as spectrum of the ^{55}Mn K_α line. The measurements were performed at a cryostat temperature of $T = 7\,\mathrm{mK}$ using field generating persistent current of $I_0 = 160\,\mathrm{mA}$. Each solid lines represents a Gaussian energy distribution with a FWHM width that is given in the figure for both histograms.

of $\tau_{\mathrm{decay}} = 240\,\mu\mathrm{s}$. Both, the signal height as well as the rather short decay time indicate that the operation temperature of the detector is higher than the cryostat temperature. By subsequently switching on and off neighboring detector channels as well as by varying the bias conditions of each detector we determined that Joule heating of the detector SQUIDs prevents the detector array to reach the cryostat temperature. We are therefore presently redesigning the array and particularly the thermalization of the shunt resistors to minimize the effect of SQUID Joule heating on the temperature sensor. Fig. 3 also shows that the signal rise is linear rather than exponential as expected from the thermodynamic model describing an MMC [5]. This indicates that slew rate of the SQUID readout limits the signal rise for the present setup.

Fig. 4 shows the energy distribution of baseline signals as well as the spectrum of the ^{55}Mn K_α line. By fitting a Gaussian function to the measured lines we extracted an energy resolution of $4.2\,\mathrm{eV}$ at $0\,\mathrm{keV}$ and $17.7\,\mathrm{eV}$ at $5.9\,\mathrm{keV}$. The baseline resolution is consistent with the independently measured detector temperature of about $50\,\mathrm{mK}$ and indicate it can be improved by enhancing the thermalization of the detector (see above). The degradation of the energy resolution for $5.9\,\mathrm{keV}$ photons is related to reaching the slew rate limit of the SQUID setup, temperature fluctuations of the experimental platform as well as a remaining athermal phonon loss due to the need for using stems with a rather large diameter. All these issues are address during the present phase of detector redesigning.

V. Summary

We have developed a prototype 64 pixels detector array based on metallic magnetic calorimeter with direct sensor readout for which the temperature sensor is placed directly into the SQUID loop. Each detector relies on a first-order parallel gradiometric SQUID formed by two meander-shaped coils onto which planar temperature sensor made of Ag:Er as well as particle absorbers made of electroplated Au are deposited. The measured pulse height for a $5.9\,\mathrm{keV}$ photon is $0.6\,\Phi_0$ at a cryostat temperature of $7\,\mathrm{mK}$. The measured baseline resolution is about $4\,\mathrm{eV}$ (FWHM). It is limited by the detector temperature which is increased compared to the cryostat temperature due to SQUID Joule heating. The measured instrumental energy resolution at $5.9\,\mathrm{keV}$ is about $18\,\mathrm{eV}$ (FWHM) and is degraded compared to the baseline resolution due to temperature fluctuations, athermal phonons loss and reaching the slew-rate limit of the SQUID readout. Presently, a revised detector version is under development having the potential to reach sub-eV energy resolution.

References

[1] S.Kempf, A. Fleischmann, L. Gastaldo, and C. Enss, J. Low Temp. Phys., vol. 193, pp. 365–379, 2018.
[2] V. Zakosarenko, R. Stolz, L. Fritzsch, H.-G. Meyer, A. Fleischmann, and C Enss, Supercond. Sci. Technol., vol. 16, pp. 1404–1407, 2003.
[3] R. Stolz, V. Zakosarenko, L. Fritzsch, H.-G. Meyer, A. Fleischmann, and C. Enss, IEEE Trans. Appl. Supercond., vol. 15, pp. 773–776, 2005.
[4] S. T. P. Boyd, R. Cantor, V. Kotsubo, P. Blumenfeld, and J. A. Hall, J. Low Temp. Phys., vol. 151, pp. 369-374, 2008.
[5] A. Fleischmann, C. Enss, G. M. Seidel, in C. Enss (eds) Cryogenic Particle Detection, Topics in Applied Physics, vol. 99. Springer, Berlin, Heidelberg, 2005.